AGU PUBLICATIONS

Geophysical Research Letters

RESEARCH LETTER
10.1002/2017GL074943

Key Points:
- Simulations of basal melt and shelf circulation before and after the Mertz Glacier Tongue (MGT) calving are compared
- Changes in the regional icescape allow warmer water to enter the ice shelf cavity increasing the MGT basal mass loss by 57% at depth
- Changes in icescape influence shelf circulation and ocean-ice shelf interactions, but the response depends on the local factors

Supporting Information:
- Supporting Information S1

Correspondence to:
E. A. Cougnon,
eva.cougnon@utas.edu.au

Citation:
Cougnon, E. A., Galton-Fenzi, B. K., Rintoul, S. R., Legrésy, B., Williams, G. D., Fraser, A. D., & Hunter, J. R. (2017). Regional changes in icescape impact shelf circulation and basal melting. *Geophysical Research Letters*, *44*. https://doi.org/10.1002/2017GL074943

Received 14 JUL 2017
Accepted 24 OCT 2017
Accepted article online 2 NOV 2017

Regional Changes in Icescape Impact Shelf Circulation and Basal Melting

E. A. Cougnon[1,2], B. K. Galton-Fenzi[2,3], S. R. Rintoul[2,4,5], B. Legrésy[2,4], G. D. Williams[1,2], A. D. Fraser[2], and J. R. Hunter[2]

[1]Institute for Marine and Antarctic Studies, University of Tasmania, Hobart, Tasmania, Australia, [2]Antarctic Climate and Ecosystems Cooperative Research Centre, Hobart, Tasmania, Australia, [3]Australian Antarctic Division, Kingston, Tasmania, Australia, [4]Ocean and Atmosphere, Commonwealth Scientific and Industrial Research Organisation, Hobart, Tasmania, Australia, [5]Centre for Southern Hemisphere Oceans Research, Hobart, Tasmania, Australia

Abstract Ice shelf basal melt is the dominant contribution to mass loss from Antarctic ice shelves. However, the sensitivity of basal melt to changes in icescape (grounded icebergs, ice shelves, and sea ice) and related ocean circulation is poorly understood. Here we simulate the impact of the major 2010 calving event of the Mertz Glacier Tongue (MGT), East Antarctica, and related redistribution of sea ice and icebergs on the basal melt rate of the local ice shelves. We find that the position of the grounded tabular iceberg B9B controls the water masses that reach the nearby ice shelf cavities. After the calving of the MGT and the removal of B9B, warmer water is present both within the MGT cavity and on the continental shelf driving a 57% increase of the deep MGT basal melting. Major changes in icescape influence the oceanic heat flux responsible for basal ice shelf melting.

1. Introduction

The Antarctic Ice Sheet has a potential contribution to global sea level rise of 58 m (Fretwell et al., 2013) and is restrained by the floating ice shelves around the continent. Ice shelf mass loss, through calving and basal melting, can lead to decreased buttressing and dynamic changes to the upstream ice sheet at different rates for each Antarctic ice shelf (Fürst et al., 2016). Most of the Antarctic Ice Sheet grounded below sea level (marine-based ice) is in East Antarctica, and its melting would raise sea level by 19 m, five times larger than for West Antarctica (Fretwell et al., 2013). The Wilkes Basin near the Mertz Glacier Tongue (MGT) has a marine-based ice equivalent to a global sea level rise of 3–4 m (Mengel & Levermann, 2014). Variability of ice shelf basal melting and input of glacial meltwater into the ocean can also influence water mass properties on the Antarctic continental shelf.

The Adélie and George V Land coast (AGVL; 136–148°E) is one of the most monitored regions in East Antarctica with many studies covering the MGT (e.g., Giles, 2017; Legrésy et al., 2004; Lescarmontier et al., 2015; Massom et al., 2015; Mayet et al., 2013), the polynya distribution (e.g., Dragon et al., 2014; Fogwill et al., 2016; Massom et al., 2001; Tamura et al., 2012), the local bathymetry (e.g., Beaman et al., 2011), and the ocean circulation (e.g., Lacarra et al., 2014; Martin et al., 2017; Shadwick et al., 2013; Snow et al., 2016; Williams et al., 2008, 2010). Prior to the MGT calving, the AGVL region had the second highest sea ice production along the East Antarctic coast (Tamura et al., 2016), partly due to the presence of the MGT and other icebergs in the area (e.g., B9B iceberg) which formed barriers to westward moving sea ice within the Antarctic coastal current (Barber & Massom, 2007). This large polynya region is of global importance because brine rejection associated with enhanced sea ice growth produces Dense Shelf Water (DSW) that contributes to Antarctic Bottom Water (AABW) (e.g., Rintoul, 1998). Previous modeling studies have highlighted the impact of interannual variability in local sea ice production on DSW production and basal ice shelf melting before the calving event (Cougnon et al., 2013; Kusahara et al., 2017; Marsland et al., 2004).

In February 2010, the MGT calved and reduced in length by about half (Figure 1). The calving of the MGT led to a dramatic change in the local icescape (icebergs, ice shelves, and sea ice) (Lescarmontier et al., 2015; Massom et al., 2015; Mayet et al., 2013). The regional polynya area west of the MGT decreased by ~70% (Dragon et al., 2014) and the 2012 sea ice production for the AGVL region (east and west of the MGT) decreased by ~21% (Tamura et al., 2016), leading to an observed freshening and a decrease in density of DSW on the continental

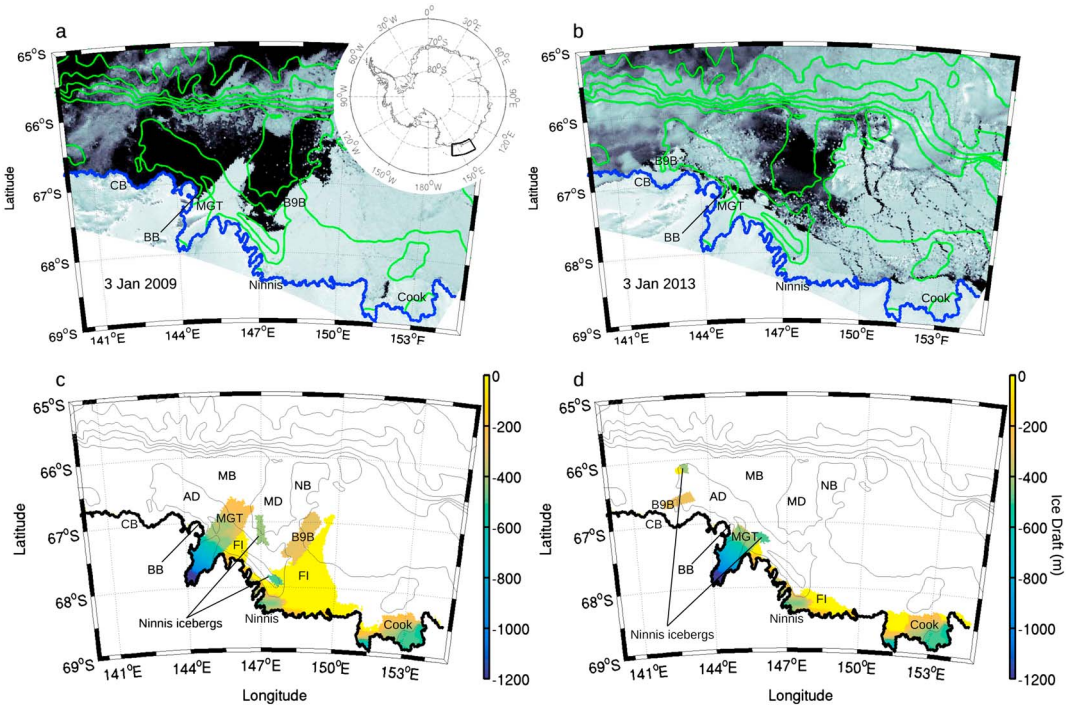

Figure 1. MODIS (Moderate Resolution Imaging Spectroradiometer) image of the MGT region (a) precalving (3 January 2009) and (b) postcalving (3 January 2013). The coastline from the model is highlighted in blue, and the bathymetry contours every 500 m in green. The ice draft (m) used in the model is shown for the (c)precalving and (d) postcalving simulation. The same coastline and bathymetry contours as in Figures 1a and 1b are shown in Figures 1c and 1d in black and grey, respectively. Key ocean, ice, and land features referred to in the text are labeled in Figures 1c and 1d. In the ocean: Adélie Depression (AD), Mertz Bank (MB), Mertz Depression (MD), and Ninnis Bank (NB); on the ice: Mertz Glacier Tongue (MGT), fast ice in yellow (FI), and B9B iceberg; along the continent: Commonwealth Bay (CB) and Buchanan Bay (BB).

shelf (Lacarra et al., 2014; Shadwick et al., 2013). The calving event makes this region an appropriate case study for modeling and understanding the implications of a regional change in icescape, in terms of its effect on both local ocean circulation and basal melt of the local ice shelves and icebergs.

Shelf air-sea processes are important in driving variability of the ice shelf basal melt by regulating the ocean heat content within the ice shelf cavities (e.g., Cougnon et al., 2013; Gwyther et al., 2014; Khazendar et al., 2013; St-Laurent et al., 2015). However, the effect of tabular icebergs on ocean circulation and ice shelf basal melting has been poorly explored. Several studies have looked at the impact of icebergs on the broader scale and on freshwater input beyond the Antarctic continental shelf (e.g., Marsh et al., 2015; Stern et al., 2016). Regional studies have highlighted the role of grounded icebergs in enhancing sea ice production locally (e.g., Fogwill et al., 2016; Massom et al., 2001; Ohshima et al., 2013). Only a few regional studies on the continental shelf have shown the influence of changes in grounded iceberg locations on the ocean properties and ice shelf basal melting (e.g., Grosfeld et al., 2001; Nakayama et al., 2014; Robinson et al., 2010). Here we use a relatively high-resolution regional ocean model, with ocean-ice shelf thermodynamics, to investigate the impact of changes in local air-sea forcing and changes in icescape on both the basal melt rate of the local ice shelves and icebergs, and on the ocean properties on the continental shelf.

2. Model

We use a modified version of the Regional Ocean Modeling System (ROMS) (Shchepetkin & McWilliams, 2005) adapted for the MGT region, before and after the 2010 calving event (Figure 1; also see supporting information for the full domain and complementary details on the model setup — Figures S1 and Text S1). The model setup used here is similar to that described by Cougnon et al. (2013), using the same horizontal and vertical grid. The horizontal grid has a resolution of ~2.16 km near the southern boundary and ~2.88 km near the northern boundary. The vertical grid is arranged to give higher resolution at the top and bottom of the water column.

The model includes ocean-ice shelf thermodynamics described by three equations following Holland and Jenkins (1999), frazil ice thermodynamics following Galton-Fenzi et al. (2012), as used in previous studies (e.g., Cougnon et al., 2013; Gwyther et al., 2014), and a simplified analytic tidal forcing at the lateral boundaries.

The bathymetry in both simulations is based on RTopo-1 (Timmermann et al., 2010) and modified to include local high-resolution bathymetry (Beaman et al., 2011) as described in Mayet et al. (2013). The MGT and B9B iceberg ice draft, along with the underlying bathymetry, is based on an early version of the most up-to-date product by Mayet et al. (2013). Figures 1a and 1b show satellite images of the precalving and postcalving icescape configuration near the MGT. The ice draft used in the model is shown in Figures 1c and 1d. For the precalving configuration two Ninnis icebergs are defined in the model as in Cougnon et al. (2013), including one that differs from the 2009 satellite image (Figure 1a). The Ninnis iceberg directly east of the MGT in the precalving simulation left the region in the 2000s, although icebergs are regularly released from the Ninnis glacier and ground or remain alongside the MGT for several years (Massom et al., 2010). The bathymetry and ice draft used in the postcalving simulation are based on the ice shelf and iceberg configuration in 2012–2013. A climatology of "persistent" landfast sea ice (between 2010 and 2012 for the postcalving configuration) updated from Fraser et al. (2012) is also included.

The model is forced at the surface with monthly data from 2009 for the precalving simulation, and 2012 for the postcalving simulation. In the absence of a dynamic sea ice model, polynya activity is represented by forcing the surface of the ocean with heat and salt fluxes. These fluxes are calculated from sea ice production estimates from a climatology derived using Special Sensor Microwave Imager data (SSMI, Tamura et al., 2011, 2016). Surface wind stress in the model is calculated using the 10 m monthly wind record from ERA-Interim (Dee et al., 2011) from 2009 and 2012 to match the air-sea heat and salt fluxes. The same lateral boundary forcing is used in both simulations, based on the 22 year climatology (1992–2013) calculated from the ECCO2 monthly fields (Menemenlis et al., 2008; Wunsch et al., 2009). In this way, we ensure that any changes between the two simulations arise from changes in both icescape and associated change in surface forcing, rather than changes outside the AGVL region (see supporting information for details). The total run time of the model for each simulation is 33 years, using an annually repeating loop of the same lateral forcing for both simulations and an annually repeating loop of the surface forcing corresponding to each icescape. This 33 year run includes a spin-up phase of 30 years to reach equilibrium. The last 3 years of each run are averaged as a time step bin climatology (each time step of each year are averaged to get a one year climatology) for the analyses.

Previous studies have shown that this model is reliable for different areas in East Antarctica, including the AGVL region, (e.g., Cottin et al., 2012; Cougnon et al., 2013; Fogwill et al., 2016; Galton-Fenzi et al., 2012; Gwyther et al., 2014). In addition, we performed an evaluation of the model with available observations, showing that the model reproduces many aspects of the water mass structure and ocean circulation both precalving and postcalving (see supporting information).

3. Changes in Basal Melting After the 2010 Calving Event

The precalving simulation indicates a basal mass loss from the entire MGT of 5.6 ± 0.5 Gt yr^{-1} (Table 1), corresponding to an area-averaged basal melt rate of 0.93 ± 0.08 m yr^{-1} (supporting information Table S1). The postcalving simulation produces comparable MGT basal mass loss of 6.0 ± 1.0 Gt yr^{-1}, corresponding to an area-averaged basal melting of 1.7 ± 0.3 m yr^{-1}. As such, the area-averaged melt rate of the MGT increased substantially (+89%) in the postcalving simulation, as the area available for melting decreased by 42% (Table 1).

The basal melting of the MGT is spatially heterogeneous (Figures 2a and 2b). In the precalving simulation, the highest rate of basal melting occurs near the narrowest point of the embayment (up to 7.5 m yr^{-1} locally). The rate of mass loss from ice drafts deeper than 900 m is 2.16 ± 0.05 Gt yr^{-1} in the precalving simulation, corresponding to 40% of the total basal mass loss of the MGT (Table 1). Another hot spot of melting is seen at the northeastern tip of the MGT, with melt rates up to 3.1 m yr^{-1} (Figure 2a), due to direct interactions with relatively warm water. The rate of mass loss from ice drafts shallower than 300 m is 1.4 ± 0.4 Gt yr^{-1} (Table 1). Finally, refreezing occurs along the western edge of the MGT cavity in the precalving simulation.

The postcalving simulation shows a similar distribution but increased magnitude of basal melting, with the maximum melt rate (up to 11.3 m yr^{-1} locally) again at the narrowest part of the MGT embayment, and a refreezing area along the western edge of the cavity. For ice drafts deeper than 900 m, giving the same area

Table 1
Basal Mass Loss for the Precalving and Postcalving Simulations With Their Standard Deviation

Ice Shelf	Mass loss precalving (Gt yr^{-1})	Mass loss postcalving (Gt yr^{-1})	% mass loss change	% basal ice shelf area change	% area-averaged melt change
Total[a]	23.8 ± 2	20.5 ± 3	−14	−19	+7
MGT	5.6 ± 0.5	6.0 ± 1.0	+7	−42	+89
B9B	5.3 ± 0.9	0.6 ± 0.1	−89	−69	−64
Ninnis	0.6 ± 0.4	1.3 ± 0.8	+117	0	+100
Cook	7.3 ± 1.4	4.5 ± 1.7	−38	0	−37
$M^b < -900$ m	2.16 ± 0.05	3.4 ± 0.5	+57	0	+57
$-900 < M^b < -600$ m	0.86 ± 0.04	1.7 ± 0.5	+98	0	+95
$-600 < M^b < -300$ m	1.2 ± 0.2	0.88 ± 0.3	−26	−50	+49
$M^b > -300$ m	1.4 ± 0.4	0.009 ± 0.005	−99	−99	−42

[a]All the ice in the model including all ice shelves, icebergs, and fast ice. [b]MGT ice draft.

precalving and postcalving, the rate of mass loss increases by 57% (Table 1). The calving of the MGT and associated change in sea ice distribution and ocean circulation also impacts ice shelves to the east. The basal mass loss from the Ninnis Ice Shelf (Figure 2) doubles after calving but remains relatively low (<1.5 Gt yr^{-1}; Table 1). In contrast, the mass loss from the Cook Ice Shelf, near the southeastern corner of the model domain, decreases by 38%, and there is no significant change in total averaged basal mass loss (Table 1).

In our model, the basal melting is parameterised via the three-equation method (Holland & Jenkins, 1999), using a velocity-dependent formulation for the estimation of heat and salt fluxes at the ocean-ice shelf interface (Gwyther et al., 2015). As a result, the basal melt rate in our model is a function of both the friction velocity (u_*) and the thermal forcing (T_*). Estimation of u_* and T_* for the ice deeper than 600 m for the MGT (same area precalving and postcalving within the embayment) shows that T_* increases by 39% between the precalving and the postcalving simulations, while u_* increases by 26%, illustrating that the increase in ocean temperature is the main driver of the 69% increase in area-averaged basal melt rate of the MGT for ice deeper than 600 m (supporting information Text S2 and Table S2).

The effect of the large tabular iceberg B9B on the area has been poorly studied. B9B rested for ~20 years on the Ninnis Bank (Mayet et al., 2013), forming a barrier against westward moving sea ice (Massom et al., 2001) and allowing a small polynya area in its lee (western side) (Massom, 2003). In our simulations, B9B iceberg precalving shows significant basal mass loss (5.3 ± 0.9 Gt yr^{-1}), which is of the same order as the MGT (Table 1). After calving, B9B shows a substantial decrease in basal mass loss, partly due to its ~70% decrease in area following partial breakup of the iceberg during the initial phase of the calving. In its precalving location,

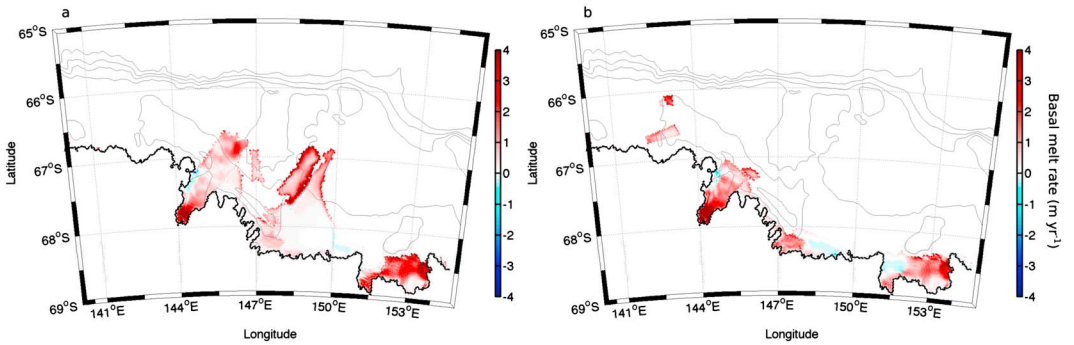

Figure 2. Time-averaged basal melting (m yr^{-1}) for the (a) precalving and (b) postcalving simulations. Positive values of basal melting correspond to melting and negative to refreezing beneath the ice shelf. Bathymetry contours every 500 m are also shown on each panel.

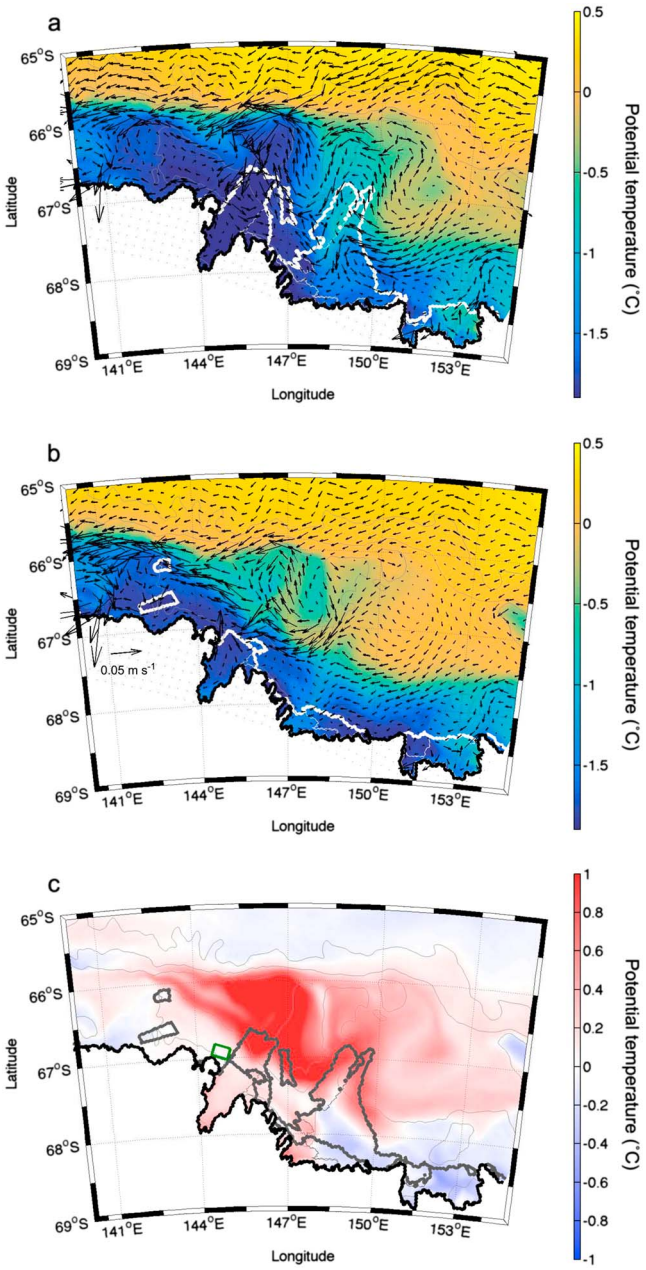

Figure 3. Time and depth-averaged potential temperature (°C) overlaid with the depth-averaged velocity field for the (a) precalving and (b) postcalving simulations. (c) The depth-averaged potential temperature difference, postcalving minus precalving. Positive values indicate warming and negative values cooling of the postcalving simulation compared to the precalving. The black contours for the three panels illustrate the coast line, and the white (grey) contours in Figures 3a and 3b (Figure 3c) illustrate the ice mask in the model and stationary ice features (icebergs, fast ice, and ice shelves).

B9B is more exposed to warmer far-field water masses than it is during postcalving, when it is grounded near the coast north of Commonwealth Bay.

4. Warmer Water on the Continental Shelf After the 2010 Calving Event

Both the ocean circulation and distribution of heat on the continental shelf change in response to the different icescape and associated surface forcing (Figure 3). In the precalving simulation, the vertically integrated ocean velocity along the shelf break and the depth-averaged potential temperature (Figure 3a) illustrate three main pathways for the modified Circumpolar Deep Water (mCDW) to flow onto the continental shelf in the MGT vicinity. One pathway is onto the Mertz Bank, allowing mCDW to interact with the northern tip of the MGT and drive high basal melt rate (Figure 2a). A second mCDW pathway is onto the Ninnis Bank. Finally, a westward flow of relatively warm mCDW ($\Theta > -1°C$), from the east of the model domain (~67.5°S, 152°E), less modified compared to the inflow via the Mertz Bank ($-1.3 < \Theta < -1°C$), is deflected by B9B (~ 67–67.5°S, 148–149°E).

In the postcalving simulation, pathways for mCDW onto the continental shelf are similar, including via the Mertz and Ninnis Banks, although the flow is generally weaker (Figures 3a and 3b). However, east of the Ninnis Bank and where the B9B iceberg was located (~67°S, 149°E), the postcalving simulation shows an intensification of the westward current. This path allows warmer mCDW ($\Theta > -0.3°C$) to flow nearer to the postcalving MGT ice front and along the southwestern flank of the Mertz Bank.

The area over the Mertz Depression and Bank (67–66°S, 144–150°E) postcalving is warmer by more than 1°C (Figure 3c), highlighting that B9B precalving redirects and modifies water masses in its lee. B9B blocks the passage of mCDW on its eastern side and leads to cooling of the water masses in its lee, both through glacial meltwater release and sea ice formation within the small polynya forming in its lee. The high melt rate of B9B precalving is a consequence of mCDW interacting mainly along its eastern and northwestern flanks (Figure 2a).

Postcalving, B9B no longer provides a barrier to restrict the inflow of warm waters from the east across the Ninnis Bank, Mertz Depression, and along the southern flank of the Mertz Bank. The remnant B9B is currently located north of Commonwealth Bay, directly west of the coastal Mertz Glacier Polynya (MGP) and away from relatively warm water circulation.

Within the deepest part of the Adélie Depression west of the MGT, the ocean circulation and potential temperature are essentially unchanged postcalving (Figures 3a and 3b). The depth-averaged potential temperature is close to the surface freezing temperature, suggesting that the wintertime convection due to polynya activity is still strong enough after calving to mix the whole water column. However, the bottom layer of the model (not shown) has freshened by 0.101 ± 0.003 within the deepest part of Adélie Depression north of Buchanan Bay (green box in Figure 3c), likely in response to the decreased sea ice formation and associated brine rejection.

The decrease in sea ice production is given in the model by a 52% decrease in salt flux input into the ocean for the green square area in Figure 3c. This decrease in salt input reduces the strength of winter convection. The related freshening signal north of Buchanan Bay is in good agreement with observations taken in 2010 and 2012, which show a decrease in bottom salinity of 0.12 (Lacarra et al., 2014). Shadwick et al. (2013)

use three years precalving (1978, 2001, and 2008) and 2012 postcalving for a similar area, finding a decrease in bottom salinity ranging from 0.08 to 0.15.

5. Discussion

The increase in area-averaged basal melt rate of the MGT after calving should imply a drop in surface elevation of the glacier after several years, assuming a constant ice velocity toward the ocean. The increase in area-averaged basal melt of ice deeper than 900 m of ~1.8 m yr^{-1}, suggests a drop in surface elevation of ~18 cm yr^{-1} after calving. Unfortunately, the currently available satellite data do not allow changes to be estimated with sufficient accuracy. The two main satellites present before calving, ICESat and ENVISAT, ended their exact repeat operations in 2009 and 2010, respectively. There is no digital elevation model (either stereo-optical or INSAR based) with the required and repeated accuracy over the period. Cryosat-2 detects a slight but not significant elevation decrease in the area (Helm et al., 2014). In the coming years a significant thinning signal may be revealed with the continuation of Cryosat-2 and the introduction of Sentinel-3 data.

A recent modeling study of the region (Kusahara et al., 2017) find that basal melting of the MGT reduces, and bottom salinity in the MGP increases associated with a decrease in bottom potential temperature, after calving, in contrast with our results and with observations of freshening and no change in potential temperature of bottom waters (Lacarra et al., 2014; Shadwick et al., 2013). Both models find an increased signal of mCDW on the shelf east of the MGT after calving, however, in Kusahara et al. (2017) this signal also explains the increase in bottom salinity in the MGP. The two models differ in several important respects. The global coupled ocean-sea ice model of Kusahara et al. (2017) has coarser horizontal resolution (5–6 km in the AGVL region); their simulated sea ice production rates are higher than the Tamura et al. (2008) estimates; they use different bathymetry and ice draft; and their ocean-ice shelf parameterization is independent of velocity and depends only on temperature. All of these factors may influence the modeled response to calving of the MGT. Few studies have shown the importance of friction velocity in the spatial distribution of the ice shelf basal melt when using a velocity-dependent formulation (e.g., Dansereau et al., 2014; Gwyther et al., 2015, 2016). Dinniman et al. (2016) highlighted the need for high horizontal resolution and a realistic shape of the ice shelf cavity. The topography of the ice shelf cavity influences the magnitude of the melt rate (Holland et al., 2008; Little et al., 2009), in particular near the grounding line as shown by plume model studies (e.g., Jenkins, 2011). The difference in ice draft may be of particular importance. In their model, ice drafts are limited to depths of 550 m, while we show that mass loss at depths (>600 m) is significant (Table 1).

Observational study by Aoki et al. (2017) shows changes in oceanic conditions after the MGT calving, with a decrease in mCDW west of the MGT but an increase east of the MGT. They also observe an increase in continental meltwater signal within the Adélie depression but they cannot clearly identify the source. They use Kusahara et al. (2017) to justify that continental meltwater may come from further east (West Antarctic Ice Sheet). However, other possible sources might be more local, such as from the Ninnis Ice Shelf just east of the MGT (further discussion in supporting information).

Here we show that B9B, in its precalving position, blocks warm waters from reaching the MGT and releases relatively high amounts of glacial meltwater (Table 1). Grosfeld et al. (2001) show that icebergs grounded in front of the Filchner Ice Shelf can decrease the thermohaline ventilation within the ice shelf cavity and subsequently decrease the ice shelf basal melting. Robinson et al. (2010) show that water masses within McMurdo Sound can be influenced by the proximity of giant icebergs allowing heavy sea ice cover and preventing warm water from accessing the ice shelf cavity. A modeling study by Nakayama et al. (2014) show that grounded icebergs west of the Pine Island (PI) Glacier act as a barrier against westward moving sea ice formed within the PI polynya, which can decrease the sea ice formation within the polynya and the associated Winter Water layer thickness, allowing mCDW to flow closer to the PI ice front. We conclude that changes in icescape can impact the basal melt of local ice shelves; however, the response varies regionally.

6. Summary

Our study highlights some consequences of regional changes in icescape (ice shelves, tabular icebergs, and sea ice) and associated changes in surface forcing on basal melting and ocean circulation. Specifically, we demonstrate that changes in location of the tabular iceberg B9B, and the calving of about half the length of the MGT, alter regional ocean currents and temperatures. This in turn leads to an increase in basal melt

of the MGT and Ninnis Ice Shelf (Table 1). Before the MGT calving, B9B redirects (by its location and thickness, Figure 3) and modifies (by releasing large amount of glacial meltwater, Table 1) the relatively warm mCDW entering the continental shelf along the AGVL region, altering the water masses reaching the ice shelf cavities.

Associated with the MGT breakup and relocation of B9B to the west, the sea ice conditions change, and the brine rejection significantly decreases leading to the presence of a fresher bottom water mass within the Adélie depression, in agreement with hydrographic measurements. In parallel, the column-averaged ocean warms to the north and northeast of the MGT by more than 1°C (Figure 3), providing a source of warmer water into the MGT cavity and driving a 57% increase in the basal mass loss for ice deeper than 900 m.

Iceberg calving events may increase in frequency with enhanced ocean-driven basal melt of Antarctic Ice Shelves (Liu et al., 2015). Our results suggest that increased numbers of large tabular icebergs, with sufficient thickness to ground on the continental shelf, will influence ocean circulation and heat transport, and hence the rate of basal melt of local ice shelves. In the Mertz region, the combined effects of drifting and regrounding of iceberg B9B and the calving of the MGT increase the rate of basal melt. Studies in other regions have found that grounding of icebergs can reduce the rate of basal melt of nearby ice shelves (e.g., Grosfeld et al., 2001; Robinson et al., 2010). We conclude that ocean-ice shelf interaction is sensitive to changes in the regional icescape, including changes precipitated by calving, drift, and grounding of large icebergs, but that the nature of the response will depend on local factors including bathymetry and the location of icebergs relative to ice shelves and ocean currents, and associated changes in air-sea fluxes.

Acknowledgments
We thank David Gwyther (Antarctic Climate and Ecosystems Cooperative Research Centre (ACE-CRC)) and Robert Massom (Australian Antarctic Division) for their insightful comments on the manuscript, and Takeshi Tamura (National Institute of Polar Research) for providing the surface heat and salt fluxes used to configure the model. We also thank two anonymous reviewers for their constructive comments on the manuscript. This work was supported in part by the Australian Government's Cooperative Research Centre Program through the ACE-CRC, by the Earth System and Climate Change Hub of the National Environmental Science Program, and by the Centre for Southern Hemisphere Ocean Research, a joint research centre of Qingdao National Laboratory for Marine Science and Technology and CSIRO. Eva Cougnon was supported by the University of Tasmania and CSIRO through the Quantitative Marine Science PhD program. Ben Galton-Fenzi and David Gwyther are supported under the Australian Research Councils Special Research Initiative for the Antarctic Gateway Partnership SRI40300001. Ben Galton-Fenzi is also supported by the Australian Antarctic Science program AAS4287. Guy Williams is supported by the Australian Research Council's "Future Fellowship" program. This work also contributes to the World Climate Research Programme (WCRP) Climate and Cryosphere (CliC) project Targeted Activity "Linkages Between Cryosphere Elements." Computing hours were provided by both the Tasmanian Partnership for Advanced Computing (TPAC) and the Australian National Computing Infrastructure (NCI) under grants m68 and gh8 and analyzed and stored on the TPAC cluster. The model raw output are difficult to make publicly available. The authors recommend contacting the corresponding author for accessing the data if interested.

References

Aoki, S., Kobayashi, R., Rintoul, S. R., Tamura, T., & Kusahara, K. (2017). Changes in water properties and flow regime on the continental shelf off the Adélie/George V Land coast, East Antarctica, after glacier tongue calving. *Journal of Geophysical Research: Oceans*, *122*, 6277–6294. https://doi.org/10.1002/2017JC012925

Barber, D., & Massom, R. (2007). A bi-polar assessment of modes of polynya formation, *Polynyas: Windows to the World* (pp. 1–54). Amsterdam: Elsevier. https://doi.org/10.1016/S0422-9894(06)74001-6

Beaman, R. J., O'Brien, P. E., Post, A. L., & Santis, L. D. (2011). A new high-resolution bathymetry model for the Terre Adélie and the George V continental margin, East Antarctica. *Antarctic Science*, *23*, 95–103. https://doi.org/10.1017/S095410201000074X

Cottin, J., Raymond, B., Kato, A., Amélineau, F., Maho, Y. L., Raclot, T., … Ropert-Coudert, Y. (2012). Foraging strategies of male Adélie penguins during their first incubation trip in relation to environmental conditions. *Marine Biology*, *159*, 1843–1852. https://doi.org/10.1007/s00227-012-1974-x

Cougnon, E. A., Galton-Fenzi, B. K., Meijers, A. J. S., & Legrésy, B. (2013). Modeling interannual dense shelf water export in the region of the Mertz Glacier Tongue (1992–2007). *Journal of Geophysical Research: Oceans*, *118*, 5858–5872. https://doi.org/10.1002/2013JC008790

Dansereau, V., Heimbach, P., & Losch, M. (2014). Simulation of subice shelf melt rates in a general circulation model: Velocity-dependent transfer and the role of friction. *Journal of Geophysical Research: Oceans*, *119*, 1765–1790. https://doi.org/10.1002/2013JC008846

Dee, D., Uppala, S., Simmons, A., Berrisford, P., Poli, P., Kobayashi, S., … Vitart, F. (2011). The ERA-Interim reanalysis: Configuration and performance of the data assimilation system. *Quarterly Journal of the Royal Meteorological Society*, *137*(656), 553–597. https://doi.org/10.1002/qj.828

Dinniman, M. S., Asay-Davis, X. S., Galton-Fenzi, B., Holland, P. R., Jenkins, A., & Timmermann, R. (2016). Modeling ice shelf/ocean interaction in Antarctica: A review. *Oceanography*, *29*(4), 144–153. https://doi.org/10.5670/oceanog.2016.106

Dragon, A.-C., Houssais, M.-N., Herbaut, C., & Charrassin, J.-B. (2014). A note on the intraseasonal variability in an Antarctic polynia: Prior to and after the Mertz Glacier calving. *Journal of Marine Systems*, *130*, 46–55. https://doi.org/10.1016/j.jmarsys.2013.06.006

Fogwill, C. J., van Sebille, E., Cougnon, E. A., Turney, C. S., Rintoul, S. R., Galton-Fenzi, B. K., … Carter, L. (2016). Brief communication: Impacts of a developing polynya off Commonwealth Bay, East Antarctica, triggered by grounding of iceberg B09B. *The Cryosphere*, *10*(6), 2603–2609. https://doi.org/10.5194/tc-10-2603-2016

Fraser, A. D., Massom, R. A., Michael, K. J., Galton-Fenzi, B. K., & Lieser, J. L. (2012). East Antarctic landfast sea ice distribution and variability, 2000–08. *Journal of Climate*, *25*(4), 1137–1156. https://doi.org/doi.org/10.1175/JCLI-D-10-05032.1

Fretwell, P., Pritchard, H. D., Vaughan, D. G., Bamber, J. L., Barrand, N. E., Bell, R., … Zirizzotti, A. (2013). Bedmap2: Improved ice bed, surface and thickness datasets for Antarctica. *The Cryosphere*, *7*(1), 375–393. https://doi.org/10.5194/tc-7-375-2013

Fürst, J. J., Durand, G., Gillet-Chaulet, F., Tavard, L., Rankl, M., Braun, M., & Gagliardini, O. (2016). The safety band of Antarctic ice shelves. *Nature Climate Change*, *6*(5), 479–482. https://doi.org/10.1038/nclimate2912

Galton-Fenzi, B. K., Hunter, J. R., Coleman, R., Marsland, S. J., & Warner, R. (2012). Numerical modelling of melt/freeze beneath the Amery ice shelf. *Journal of Geophysical Research*, *117*, C09031. https://doi.org/10.1029/2012JC008214

Giles, A. (2017). The Mertz Glacier Tongue, East Antarctica. Changes in the past 100 years and its cyclic nature-Past, present and future. *Remote Sensing of Environment*, *191*, 30–37. https://doi.org/10.1016/j.rse.2017.01.003

Grosfeld, K., Schröder, M., Fahrbach, E., Gerdes, R., & Mackensen, A. (2001). How iceberg calving and grounding change the circulation and hydrography in the Filchner Ice Shelf-Ocean System. *Journal of Geophysical Research*, *106*(C5), 9039—9055. https://doi.org/10.1029/2000JC000601

Gwyther, D. E., Cougnon, E. A., Galton-Fenzi, B. K., Roberts, J. L., Hunter, J. R., & Dinniman, M. S. (2016). Modelling the response of ice shelf basal melting to different ocean cavity environmental regimes. *Annals of Glaciology*, *57*(73), 131–141. https://doi.org/10.1017/aog.2016.31

Gwyther, D. E., Galton-Fenzi, B. K., Dinniman, M. S., Roberts, J. L., & Hunter, J. R. (2015). The effect of basal friction on melting and freezing in ice shelf-ocean models. *Ocean Modelling*, *95*, 38–52. https://doi.org/10.1016/j.ocemod.2015.09.004

Gwyther, D., Galton-Fenzi, B., Hunter, J., & Roberts, J. (2014). Simulated melt rates for the Totten and Dalton ice shelves. *Ocean Science*, *10*(3), 267. https://doi.org/10.5194/os-10-267-2014

Helm, V., Humbert, A., & Miller, H. (2014). Elevation and elevation change of Greenland and Antarctica derived from CryoSat-2. *The Cryosphere*, *8*(4), 1539–1559. https://doi.org/10.5194/tc-8-1539-2014

Holland, D. M., & Jenkins, A. (1999). Modelling thermodynamic ice ocean interactions at the base of an ice shelf. *Journal of Physical Oceanography*, *29*, 1787–1800.

Holland, P. R., Jenkins, A., & Holland, D. M. (2008). The response of ice shelf basal melting to variations in ocean temperature. *Journal of Climate*, *21*(11), 2558–2572. https://doi.org/10.1175/2007JCLI1909.1

Jenkins, A. (2011). Convection-driven melting near the grounding lines of ice shelves and tidewater glaciers. *Journal of Physical Oceanography*, *41*(12), 2279–2294. https://doi.org/10.1175/JPO-D-11-03.1

Khazendar, A., Schodlok, M. P., Fenty, I., Ligtenberg, S. R. M., Rignot, E., & van den Broeke, M. R. (2013). Observed thinning of Totten Glacier is linked to coastal polynya variability. *Nature Communications*, *4*, 2857. https://doi.org/10.1038/ncomms3857

Kusahara, K., Hasumi, H., Fraser, A. D., Aoki, S., Shimada, K., Williams, G. D., … Tamura, T. (2017). Modeling Ocean–Cryosphere Interactions off Adélie and George V Land, East Antarctica. *Journal of Climate*, *30*(1), 163–188. https://doi.org/10.1175/JCLI-D-15-0808.1

Lacarra, M., Houssais, M.-N., Herbaut, C., Sultan, E., & Beauverger, M. (2014). Dense shelf water production in the Adélie Depression, East Antarctica, 2004–2012: Impact of the Mertz Glacier calving. *Journal of Geophysical Research: Oceans*, *119*, 5203–5220. https://doi.org/10.1002/2013JC009124

Legrésy, B., Wendt, A., Tabacco, I., Rémy, F., & Dietrich, R. (2004). Influence of tides and tidal current on Mertz Glacier, Antarctica. *Journal of Glaciology*, *50*(170), 427–435. https://doi.org/10.3189/172756504781829828

Lescarmontier, L., Legrésy, B., Young, N., Coleman, R., Testut, L., Mayet, C., & Lacroix, P. (2015). Rifting processes and ice-flow modulation observed on Mertz Glacier, East Antarctica. *Journal of Glaciology*, *61*(230), 1183–1193. https://doi.org/10.3189/2015JoG15J028

Little, C. M., Gnanadesikan, A., & Oppenheimer, M. (2009). How ice shelf morphology controls basal melting. *Journal of Geophysical Research*, *114*, C12007. https://doi.org/10.1029/2008JC005197

Liu, Y., Moore, J. C., Cheng, X., Gladstone, R. M., Bassis, J. N., Liu, H., … Hui, F. (2015). Ocean-driven thinning enhances iceberg calving and retreat of Antarctic ice shelves. *Proceedings of the National Academy of Sciences of the United States of America*, *112*(11), 3263–3268. https://doi.org/10.1073/pnas.1415137112

Marsh, R., Ivchenko, V. O., Skliris, N., Alderson, S., Bigg, G. R., Madec, G., … Zalesny, V. B. (2015). NEMO-ICB (v1.0): Interactive icebergs in the NEMO ocean model globally configured at Eddy-permitting resolution. *Geoscientific Model Development*, *8*(5), 1547–1562. https://doi.org/10.5194/gmd-8-1547-2015

Marsland, S. J., Bindoff, N. L., Williams, G. D., & Budd, W. F. (2004). Modeling water mass formation in the Mertz Glacier Polynya and Adelie Depression, East Antarctica. *Journal of Geophysical Research*, *109*, C11003. https://doi.org/10.1029/2004JC002441

Martin, A., Houssais, M.-N., Goff, H. L., Marec, C., & Dausse, D. (2017). Circulation and water mass transports on the East Antarctic shelf in the Mertz Glacier region. *Deep Sea Research Part I*, *126*, 1–20. https://doi.org/10.1016/j.dsr.2017.05.007

Massom, R. A. (2003). Recent iceberg calving events in the Ninnis Glacier region, East Antarctica. *Antarctic Science*, *15*(2), 303–313.

Massom, R. A., Hill, K. L., Lytle, V. I., Worby, A. P., Paget, M. J., & Allison, I. (2001). Effects of regional fast-ice and iceberg distributions on the behaviour of the Mertz Glacier polynya, East Antarctica. *Annals of Glaciology*, *33*, 391–398.

Massom, R. A., Giles, A. B., Fricker, H. A., Warner, R. C., Legrésy, B., & Hyland, G. (2010). Examining the interaction between multi-year landfast sea ice and the Mertz Glacier Tongue, East Antarctica: Another factor in ice sheet stability? *Journal of Geophysical Research*, *115*, C12027. https://doi.org/10.1029/2009JC006083

Massom, R. A., Giles, A. B., Warner, R. C., Fricker, H. A., Legrésy, B., & Hyland, G. (2015). External influences on the Mertz Glacier Tongue (East Antarctica) in the decade leading up to its calving in 2010. *Journal of Geophysical Research: Earth Surface*, *120*, 490–506. https://doi.org/10.1002/2014JF003223

Mayet, C., Testut, L., Legrésy, B., Lescarmontier, L., & Lyard, F. (2013). High-resolution barotropic modeling and the calving of the Mertz Glacier, East Antarctica. *Journal of Geophysical Research: Oceans*, *118*, 5267–5279. https://doi.org/10.1002/jgrc.20339

Menemenlis, D., Campin, J. M., Heimbach, P., Hill, C., Lee, T., Nguyen, A., … Zhang, H. (2008). ECCO2: High resolution global ocean and sea ice data synthesis. *Mercator Ocean Quarterly Newsletter*, *31*, 13–21.

Mengel, M., & Levermann, A. (2014). Ice plug prevents irreversible discharge from East Antarctica. *Nature Climate Change*, *4*, 451–455. https://doi.org/10.1038/nclimate2226

Nakayama, Y., Timmermann, R., Schröder, M., & Hellmer, H. H. (2014). On the difficulty of modeling Circumpolar Deep Water intrusions onto the Amundsen Sea continental shelf. *Ocean Modelling*, *84*, 26–34. https://doi.org/10.1016/j.ocemod.2014.09.007

Ohshima, K. I., Fukamachi, Y., Williams, G. D., Nihashi, S., Roquet, F., Kitade, Y., … Wakatsuchi, M. (2013). Antarctic Bottom Water production by intense sea-ice formation in the Cape Darnley polynya. *Nature Geoscience*, *6*, 235–240. https://doi.org/10.1038/ngeo1738

Rintoul, S. (1998). On the origin and influence of Adélie Land Bottom Water. In S. S. Jacobs & R. F. Weiss (Eds.), *Ocean, ice, and atmosphere: Interaction at the Antarctic Continental Margin, Antarctic Research Series* (pp. 151–172). Washington, DC: American Geophysical Union. https://doi.org/10.1029/AR075p0151

Robinson, N. J., Williams, M. J. M., Barrett, P. J., & Pyne, A. R. (2010). Observations of flow and ice-ocean interaction beneath the McMurdo ice shelf, Antarctica. *Journal of Geophysical Research*, *115*, C03025. https://doi.org/10.1029/2008JC005255

Shadwick, E. H., Rintoul, S. R., Tilbrook, B., Williams, G. D., Young, N., Fraser, A. D., … Tamura, T. (2013). Glacier tongue calving reduced dense water formation and enhanced carbon uptake. *Geophysical Research Letters*, *40*, 904–909. https://doi.org/10.1002/grl.50178

Shchepetkin, A. F., & McWilliams, J. C. (2005). The Regional Oceanic Modeling system (ROMS): A split-explicit, free-surface, topography-following-coordinate oceanic model. *Ocean Modelling*, *9*, 347–404. https://doi.org/10.1016/j. ocemod.2004.08.002

Snow, K., Sloyan, B., Rintoul, S., Hogg, A., & Downes, S. (2016). Controls on circulation, cross-shelf exchange and dense water formation in an Antarctic polynya. *Geophysical Research Letters*, *43*, 7089–7096. https://doi.org/10.1002/2016GL069479

St-Laurent, P., Klinck, J., & Dinniman, M. (2015). Impact of local winter cooling on the melt of Pine Island Glacier, Antarctica. *Journal of Geophysical Research: Oceans*, *120*, 6718–6732. https://doi.org/10.1002/2015JC010709

Stern, A. A., Adcroft, A., & Sergienko, O. (2016). The effects of Antarctic iceberg calving-size distribution in a global climate model. *Journal of Geophysical Research: Oceans*, *121*, 5773–5788. https://doi.org/10.1002/2016JC011835

Tamura, T., Ohshima, K. I., Fraser, A. D., & Williams, G. D. (2016). Sea ice production variability in Antarctic coastal polynyas. *Journal of Geophysical Research: Oceans*, *121*, 2967–2979. https://doi.org/10.1002/2015JC011537

Tamura, T., Ohshima, K. I., & Nihashi, S. (2008). Mapping of sea ice production for Antarctic coastal polynyas. *Geophysical Research Letters*, *35*, L0760. https://doi.org/10.1029/2007GL032903

Tamura, T., Ohshima, K. I., Nihashi, S., & Hasumi, H. (2011). Estimation of surface heat/salt fluxes associated with sea ice growth/melt in the southern ocean. *SOLA*, *7*, 17–20. https://doi.org/10.2151/sola.2011-005

Tamura, T., Williams, G. D., Frazer, A. D., & Ohshima, K. I. (2012). Potential regime shift in decreased sea ice production after the Mertz Glacier calving. *Nature Communications*, *3*, 826. https://doi.org/10.1038/ncomms1820

Timmermann, R., Brocq, A. L., Deen, T., Domack, E., Dutrieux, P., Galton-Fenzi, B., … Smith, W. H. F. (2010). A consistent dataset of Antarctic ice sheet topography, cavity geometry, and global bathymetry. *Earth System Science Data*, *3*, 231–257. https://doi.org/10.5194/essd-2-261-2010

Williams, G. D., Aoki, S., Jacobs, S. S., Rintoul, S. R., Tamura, T., & Bindoff, N. L. (2010). Antarctic Bottom Water from the Adélie and George V Land coast, East Antarctica (140–149°E). *Journal of Geophysical Research*, *115*, C04027. https://doi.org/10.1029/2009JC005812

Williams, G. D., Bindoff, N. L., Marsland, S. J., & Rintoul, S. R. (2008). Formation and export of dense shelf water from the Adélie Depression, East Antarctica. *Journal of Geophysical Research*, *113*, 4039. https://doi.org/10.1029/2007JC004346

Wunsch, C., Heimbach, P., Ponte, R. M., Fukumori, I., & ECCO-GODAE Consortium Members (2009). Global general circulation of the ocean estimated by the ECCO-consortium. *Oceanography*, *22*, 88–103.

Supporting Information for "Regional changes in icescape impact shelf circulation and basal melting"

E. A. Cougnon[1,2], B. K. Galton-Fenzi[2,3], S. R. Rintoul[2,4,5], B. Legrésy[2,4],G. D. Williams[1,2], A. D. Fraser[2], J. R. Hunter[2]

Corresponding author: E. A. Cougnon, Institute for Marine and Antarctic Studies, University of Tasmania, Private Bag 129, Hobart, TAS 7001, Australia. (eva.cougnon@utas.edu.au)

[1]Institute for Marine and Antarctic Studies, University of Tasmania, Hobart, Australia

[2]Antarctic Climate & Ecosystems Cooperative Research Centre, Hobart, Australia

[3]Australian Antarctic Division, Kingston, Australia

[4]Commonwealth Scientific and Industrial Research Organisation, Ocean & Atmosphere, Hobart, Australia

[5]Centre for Southern Hemisphere Oceans Research, Hobart, Australia

Contents of this file

1. Text S1 to S3
2. Figures S1 to S3
3. Tables S1 to S2

Introduction

The supporting information within this document provides additional information about the model setup and domain, including details on the velocity-dependent formulation used for estimation of heat and salt fluxes at the ocean-ice shelf interface. Additional values for basal melting and mass loss are provided, and values of thermal forcing and friction velocity from the Mertz Glacier Tongue (MGT). Model fields are also compared with observations.

Text S1. Model setup

The model used in this study is a modified version of the Regional Ocean Modeling System (ROMS) [*Shchepetkin and McWilliams*, 2005] adapted for the MGT region, before and after the 2010 calving event (Figure S1). The model setup used here is similar to that described by *Cougnon et al.* [2013], using the same horizontal and vertical grid. 31 terrain following levels are used with higher vertical resolution at the top and bottom. Cell thicknesses for the upper, mid-column and bottom layers are about 0.005, 0.062 and 0.017 times the water column thickness, respectively.

The simplified analytic tidal forcing is used at the lateral boundaries to exclude aliasing during analysis and allow a one year climatology forcing, with an exactly periodic tidal signal of 26 cycles for a 364 day-year in the model. The frequencies of the four main tidal constituents are adjusted to be periodic in 14 days, following a similar approach to that in *Pingree and Griffiths* [1981a, b]

- M2: 27 cycles per 14 days

- S2: 28 cycles per 14 days

- K1: 14 cycles per 14 days

- O1: 13 cycles per 14 days

These tidal constituents can be easily separated by a simple Fourier analysis, if necessary. Also, since the forcing is exactly periodic in a model year (364-day year) the aliasing due to having a non-integer number of tidal cycles per year is removed, and it is easier to repeat a one year climatology forcing at the lateral boundaries. This also implies that all the forcing must be adjusted to a 364-day model year.

The same lateral boundary forcing is used for both simulations pre- and post-calving, and comes from a 22-year climatology (1992-2013) calculated from the monthly fields from ECCO2 reanalysis [*Menemenlis et al.*, 2008; *Wunsch et al.*, 2009]. The choice to use the same lateral boundary forcing is in part because the ECCO2 reanalysis does not represent the densest AABW variety, producing a warmer and less dense AABW compared to observations, due to the relatively coarse vertical resolution used in the reanalyses [*Azaneu et al.*, 2014]. In addition, using the same lateral boundary forcing eliminates a possible source of change in the ocean circulation and basal ice shelf melting.

Our focus here is on the effect of a regional change in icescape, including change in ice shelf, icebergs and sea ice production, on the local basal ice shelf melting and ocean circulation on the continental shelf.

Heat and salt fluxes are prescribed at the surface of the ocean, instead of using a dynamic sea ice model to resolve the fine-scale polynya activity. These fluxes are derived from sea ice concentration using Special Sensor Microwave Imager data (SSM/I – *Tamura et al.* [2011]; *Tamura et al.* [2016]). Modifications were made to the transfer of heat and salt during the freezing season for reasons described below and in *Cougnon* [2016].

During winter (freezing season), negative heat flux (ocean losing heat to the atmosphere) is set to zero when the uppermost ocean layer temperature is equal to the surface freezing temperature. This avoids cooling the surface temperature of the ocean below the surface freezing temperature. A limitation with using the *Tamura et al.* [2011]; *Tamura et al.* [2016] dataset to force our model is that during summer the positive heat flux drives high surface ocean temperatures in the model. At the start of the freezing season (autumn), negative heat flux (cooling) and positive salt flux are forced at the surface of the ocean in the same time step. In reality, the convection of cold and salty water begins in early autumn due to surface cooling. Only after the remnant heat from the summer mixed layer is eroded, does the surface layer reach the freezing point and allow sea ice to grow and reject salt into the ocean. This autumnal conditioning of the upper surface layer has been explored in the Mertz region by *Williams et al.* [2011].

In the model, salt input to the ocean occurs at the same time as the heat flux cools the surface of the ocean, without taking into consideration the sea surface temperature.

This is not an issue when the air-sea fluxes are associated with strong negative heat flux (strong and fast cooling) during the winter months. The warm surface layer is eroded in only a few model time steps. The surface of the ocean is cooled to the surface freezing temperature quickly enough to form a water mass at the surface freezing temperature with the addition of salt that can sink to the sea floor. However, this is an issue when cooling is weak. The heat flux is insufficient to cool the ocean surface to the freezing temperature and yet salt is still injected into the ocean. As a result, warmer water is convected to the sea floor, with implications for oceanic heat input to the base of the ice shelves.

To improve the ocean surface temperature and the salt flux during the freezing season, two modifications have been made in the parameterisation of the air-sea fluxes:

1. During warming (positive heat flux) the ocean surface temperature is limited to a maximum of 0 °C roughly consistent with the few observations that include surface waters [e.g. *Lacarra et al.*, 2011]

2. During freezing conditions (negative heat flux), the surface temperature must reach near the freezing point before the positive salt flux is applied: let the heat flux to cool the surface of the ocean to $T_f + 0.1$ °C before applying the prescribed salt flux (T_f is the *in situ* freezing temperature).

These two modifications are not perfect but allow the model to simulate more realistic brine rejection during the freezing season [*Cougnon*, 2016]. An issue with this parameterisation is that it may lead to an underestimate of the amount of salt injected into the ocean. Ultimately a coupled sea-ice model is needed to resolve the seasonal changes in upper ocean stratification in response to sea ice formation and melt. However, coastal

polynyas and icebergs are often poorly resolved in models, leading to large discrepancies between observed and simulated salt flux. By imposing heat and salt fluxes based on observations and reanalyses, we better resolve the fine-scale polynya in the region. A similar approach has been used in other studies [e.g. *Dinniman et al.*, 2003, 2007; *Galton-Fenzi et al.*, 2012; *Hattermann et al.*, 2014].

Text S2. Friction velocity and thermal forcing

The friction velocity in the model is calculated using the dimensionless drag coefficient ($Cd = 0.005$), that is spatially constant over the entire ice shelf, and the modeled velocity (m s^{-1}) of the top layer immediately beneath the ice shelf (U_{top}): $u_* = \sqrt{Cd} \times U_{top}$. The thermal forcing ($T_*$) is the difference between the *in-situ* temperature beneath the ice shelf and the *in-situ* freezing temperature that varies with pressure.

Text S3. Model limitations

To assess the limitations of the model, we compare the model with available observations near the MGT. The observations are sparse and were taken mainly in summer, which illustrate different snapshots of the summer conditions. We also know that the water mass distribution on the continental shelf varies from year-to-year, as seen in observations [e.g. *Shadwick et al.*, 2013; *Lacarra et al.*, 2014] and models [*Cougnon et al.*, 2013; *Kusahara et al.*, 2017]. The model simulations presented here are driven by forcing and icescape configuration from a particular year and so we do not expect the model to reproduce the interannual variability. Previous studies have shown that this model provides realistic

simulations for different areas in East Antarctica when using realistic forcing, including the Mertz region, [e.g. *Galton-Fenzi et al.*, 2012; *Cottin et al.*, 2012; *Cougnon et al.*, 2013; *Gwyther et al.*, 2014; *Fogwill et al.*, 2016]. This section describes some of the model limitations in comparison to available sparse (in time and space) observations.

Here, we compare water mass distributions along the western edge of the pre-calving MGT (MGT west) and along the northern MGT post-calving ice front (MGT north). Figure S2 shows the locations of the Conductivity-Temperature-Depth profiler (CTD) stations from three years (August 1999, January 2001 and 2015) used to compare with the model, and the model sections used around the MGT (MGT west and MGT north sections). The observations from 2001 were measured from the RV Nathaniel B. Palmer and the other years from the RSV Aurora Australis [*Rosenberg et al.*, 2001; *Rosenberg and Rintoul*, 2015 unpublished]. These observations were already used in several studies [e.g. *Snow et al.*, 2016; *Aoki et al.*, 2017] and are available through World Ocean Database (https://www.nodc.noaa.gov/OC5/WOD/pr_wod.html) and the Australian Antarctic Data Centre (https://data.aad.gov.au/). Figure S3 shows the potential temperature and salinity along the MGT west section and the MGT north section from the model (winter and summer) and observations (August 1999 and January 2001 and 2015).

The overall stratification and water mass structure in the model is similar to the observations, both pre- and post-calving (Figure S3). Pre-calving, the model reproduces mCDW intrusions on the northern flank of the Adélie depression. However, within the depression, the model is generally fresher than the observations, as expected given the

adjustments made to the surface forcing (see Text S1 above and *Cougnon* [2016, Appendix A] for more details). Post-calving, the model simulates a similar structure to the observations of the summer water masses and a warming of the mCDW at the northern end of the MGT west section (Figure S3 c and g). However, the core of the modeled mCDW along the MGT west section in summer is warmer than observed in January 2015. In addition, the mCDW extends further south in the post-calving simulation than the summer snapshot from the 2015 observations (Figure S3 c and g). Warmer water is present in front of the northern ice front of the MGT in the post-calving simulation compared to the observations (+0.4-0.5°C, Figure S3 d and h) but is not as warm as simulated north of the MGT west section in the post-calving simulation.

Seasonal and interannual variability was observed in this region pre-calving. We expect this variability to continue post-calving, but there are no observations to confirm this. Both observations and model simulations show a strong seasonal change in the salinity of Dense Shelf Water (DSW) at the bottom of the Adélie Depression pre-calving. The salinity of DSW is lower in the model than observed, and seasonal change is a little weaker when comparing with available mooring data near the MGT pre-calving [*Williams et al.*, 2008], mainly due to the adaptation of the surface forcing described in Text S1.

The model simulations reproduce many aspects of the observed circulation, including the intrusion of mCDW over the Mertz Bank flowing to the southeast, as far as the MGT, flowing back to the northwest on the northern flank of the Adélie depression, and the transport of denser water masses to the northwest. These circulation patterns were also described in several observational studies [e.g. *Williams et al.*, 2008; *Snow et al.*, 2016;

Martin et al., 2017]. In addition, the model represents the change in seasonal circulation within the Adélie depression with a tendency for more baroclinic flow in summer and more barotropic flow in winter [*Cougnon*, 2016] as described in an observation study by *Martin et al.* [2017].

There are not enough observations at this stage to understand the velocity change post-calving. *Snow et al.* [2016] do not find significant circulation changes in summer post-calving compared to pre-calving observations. However, they find stronger differences in the seasonality as mentioned above. Another study from *Aoki et al.* [2017], suggests a decrease in mCDW import across the Mertz Bank but an increase of mCDW east of the MGT, illustrating an east-west circulation on the continental shelf. This is also seen in the model post-calving, Figure 3b in the manuscript shows weaker velocity vectors over the Mertz Bank compared to the pre-calving simulation, and a stronger inflow of mCDW east of the MGT due to the relocation of B9B iceberg. However, due to this east-west mCDW circulation, the model may over estimate the mCDW near the MGT compared to a single summer snapshot of the water mass distribution from the observations.

Aoki et al. [2017] shows an increase in the continental meltwater fraction within the Adélie depression but they cannot identify the exact source of the continental melt. In their study, they use the model study from *Kusahara et al.* [2017] to justify that the glacial meltwater is unlikely to have a local source as they model a decrease in ice shelf basal melting of the local ice shelves after calving. *Aoki et al.* [2017] propose that the increase in continental meltwater fraction found in the region could come from further east (as far as the West Antarctic Ice Sheet). Also, they argue that it is unlikely that there is

an increase of basal melt from the MGT. They do not see a significant change in oxygen isotope ratio, a proxy to identify continental meltwater fraction, between two areas pre- and post-calving where they expect the main outflow of glacial meltwater from the MGT to be located (within Buchanan Bay in the corner just west of the MGT). No change in glacial meltwater outflow would imply that the basal melting of the MGT within the embayment is of similar magnitude to pre-calving. We could also argue that meltwater from the Ninnis Ice Shelf may contribute to the increase of glacial meltwater within the Adélie depression. The observations are too sparse (in time and space) to determine the source of the increase of continental meltwater fraction within the Adélie depression, whether it is a local source or an advection of glacial meltwater from further east along the Antarctic coast.

Overall, the model does reasonably well pre-calving, including comparing the seasonal cycle to the mooring shown in *Williams et al.* [2008]. Bottom water within the Adélie depression freshens in response to the decrease in sea ice production after calving, consistent with the observations [*Shadwick et al.*, 2013; *Lacarra et al.*, 2014] but in contrast to the model of *Kusahara et al.* [2017]. The increase in bottom salinity within the Adélie depression in their model is attributed to compensation of the reduced surface salinity flux by lateral salinity flux from enhanced mCDW intrusions from the east of the MGT, associated with a decrease in bottom potential temperature [Fig. 20 in *Kusahara et al.*, 2017]. Also, here we use a spin up phase of 30 years before analyzing three more years of run. The model simulations presented here are more representative of the region in the longer term under the same surface forcing and icescape distribution. As we use the

same lateral boundary forcing and modify only the surface forcing following the change in icescape, these simulations illustrate the impact of two stable icescape configurations, and the associated changes in surface forcing, on the local oceanography. These simulations do not include any potential influence of changes in the ocean circulation over the broader region.

References

Aoki, S., R. Kobayashi, S. R. Rintoul, T. Tamura, and K. Kusahara (2017), Changes in water properties and flow regime on the continental shelf off the Adélie/George V Land coast, East Antarctica, after glacier tongue calving, *Journal of Geophysical Research: Oceans*, *122*(8), 6277–6294, doi:10.1002/2017JC012925.

Azaneu, M., R. Kerr, and M. M. Mata (2014), Assessment of the ECCO2 reanalysis on the representation of Antarctic Bottom Water properties, *Ocean science discussion*, pp. 1023–1091, doi:10.5194/osd-11-1023-2014.

Cottin, J., B. Raymond, A. Kato, F. Amélineau, Y. L. Maho, T. Raclot, B. Galton-Fenzi, A. Meijers, and Y. Ropert-Coudert (2012), Foraging strategies of male Adélie penguins during their first incubation trip in relation to environmental conditions, *Marine Biology*, doi:10.1007/s00227-012-1974-x.

Cougnon, E. A. (2016), Modelling the sensitivity of Dense Shelf Water formation in the Mertz Glacier Region, East Antarctica, Ph.D. thesis, University of Tasmania, Hobart, Tasmania, Australia.

Cougnon, E. A., B. K. Galton-Fenzi, A. J. S. Meijers, and B. Legrésy (2013), Modeling interannual dense shelf water export in the region of the Mertz Glacier Tongue

(1992–2007), *Journal of Geophysical Research: Oceans*, *118*(10), 5858–5872, doi: 10.1002/2013JC008790.

Dinniman, M. S., J. M. Klinck, and W. O. Smith Jr. (2003), Cross-shelf exchange in a model of the Ross Sea circulation and biogeochemistry, *Deep Sea Research II*, *50*, 3103–312, doi:10.1016/j.dsr2.2003.07.011.

Dinniman, M. S., J. M. Klinck, and W. O. S. Jr. (2007), Influence of sea ice cover and icebergs on circulation and water mass formation in a numerical circulation model of the Ross Sea, Antarctica, *Journal of Geophysical Research*, *112*(C1013), doi: doi:10.1029/2006JC004036.

Fogwill, C. J., E. van Sebille, E. A. Cougnon, C. S. Turney, S. R. Rintoul, B. K. Galton-Fenzi, G. F. Clark, E. Marzinelli, E. B. Rainsley, and L. Carter (2016), Brief communication: Impacts of a developing polynya off Commonwealth Bay, East Antarctica, triggered by grounding of iceberg B09B, *The Cryosphere*, *10*(6), 2603–2609, doi:10.5194/tc-10-2603-2016.

Galton-Fenzi, B. K., J. R. Hunter, R. Coleman, S. J. Marsland, and R. Warner (2012), Numerical modelling of melt/freeze beneath the Amery Ice Shelf, *Journal of Geophysical Research*, *117*(C09031), doi:10.1029/2012JC008214.

Gwyther, D., B. Galton-Fenzi, J. Hunter, and J. Roberts (2014), Simulated melt rates for the Totten and Dalton ice shelves, *Ocean Science*, *10*(3), 267, doi:10.5194/os-10-267-2014.

Hattermann, T., L. H. Smedsrud, O. A. Nøst, J. M. Lilly, and B. K. Galton-Fenzi (2014), Eddy-resolving simulations of the Fimbul Ice Shelf cavity circulation:

Basal melting and exchange with open ocean, *Ocean Modelling*, *82*, 28–44, doi: 10.1016/j.ocemod.2014.07.004.

Kusahara, K., H. Hasumi, A. D. Fraser, S. Aoki, K. Shimada, G. D. Williams, R. Massom, and T. Tamura (2017), Modeling Ocean–Cryosphere Interactions off Adélie and George V Land, East Antarctica, *Journal of Climate*, *30*(1), 163–188, doi:10.1175/JCLI-D-15-0808.1.

Lacarra, M., M.-N. Houssais, E. Sultan, S. Rintoul, and C. Herbaut (2011), Summer hydrography on the shelf off Terre Adélie/George V Land based on the ALBION and CEAMARC observations during the IPY, *Polar Science*, *5*(2), 88–103, doi: 10.1016/j.polar.2011.04.008.

Lacarra, M., M.-N. Houssais, C. Herbaut, E. Sultan, and M. Beauverger (2014), Dense shelf water production in the Adélie Depression, East Antarctica, 2004–2012: Impact of the Mertz Glacier calving, *Journal of Geophysical Research: Oceans*, *119*(8), 5203–5220, doi:10.1002/2013JC009124.

Martin, A., M.-N. Houssais, H. L. Goff, C. Marec, and D. Dausse (2017), Circulation and water mass transports on the East Antarctic shelf in the Mertz Glacier region, *Deep Sea Research Part I*, doi:10.1016/j.dsr.2017.05.007.

Menemenlis, D., J. M. Campin, P. Heimbach, C. Hill, T. Lee, A. Nguyen, M. Schodlock, and H. Zhang (2008), ECCO2: High resolution global ocean and sea ice data synthesis., *Mercator Ocean Quarterly Newsletter*, *31*, 13–21.

Pingree, R. D., and D. K. Griffiths (1981a), The N2 tide and semidiurnal amphidromes around the British Isles, *Journal of the Marine Biological Association of the United*

Kingdom, *61*, 617–625, doi:10.1017/S0025315400048086.

Pingree, R. D., and D. K. Griffiths (1981b), S2 tidal simulations on the north-west European shelf, *Journal of the Marine Biological Association of the United Kingdom*, *61*, 609–616, doi:10.1017/S0025315400048074.

Rosenberg, M., and S. Rintoul (2015 unpublished), Aurora Australis Marine Science Cruise AU1402, Totten and Mertz CTD's and Moorings - oceanographic field measurements and analysis, *Tech. rep.*, Antarctic Climate & Ecosystems Cooperative Research Centre, Hobart, Australia, 2015 unpublished report, 69 pp.

Rosenberg, M., N. Bindoff, S. Bray, C. Curran, I. Helmond, K. Miller, D. McLaughlan, and J. Richman (2001), Mertz Polynya Experiment, marine science cruises AU9807, AU9801, AU9905, AU9901 and TA0051 – oceanographic field measurements and analysis, *Tech. rep.*, Antarctic Cooperative Research Centre, Research Report No. 25, June 2001, Hobart, Australia, 89 pp.

Shadwick, E. H., S. R. Rintoul, B. Tilbrook, G. D. Williams, N. Young, a. D. Fraser, H. Marchant, J. Smith, and T. Tamura (2013), Glacier tongue calving reduced dense water formation and enhanced carbon uptake, *Geophysical Research Letters*, *40*(5), 904–909, doi:10.1002/grl.50178.

Shchepetkin, A. F., and J. C. McWilliams (2005), The Regional Oceanic Modeling system (ROMS): a split-explicit, free-surface, topography-following-coordinate oceanic model, *Ocean Modelling*, *9*, 347–404, doi:10.1016/j.ocemod.2004.08.002.

Snow, K., B. Sloyan, S. Rintoul, A. Hogg, and S. Downes (2016), Controls on circulation, cross-shelf exchange and dense water formation in an Antarctic polynya, *Geophysical*

Research Letters, *43*, doi:10.1002/2016GL069479.

Tamura, T., K. I. Ohshima, S. Nihashi, and H. Hasumi (2011), Estimation of surface heat/salt fluxes associated with sea ice growth/melt in the southern ocean, *SOLA*, *7*, 17–20, doi:10.2151/sola.2011-005.

Tamura, T., K. I. Ohshima, A. D. Fraser, and G. D. Williams (2016), Sea ice production variability in Antarctic coastal polynyas, *Journal of Geophysical Research: Oceans*, doi:10.1002/2015JC011537.

Williams, G. D., N. L. Bindoff, S. J. Marsland, and S. R. Rintoul (2008), Formation and export of dense shelf water from the Adélie Depression, East Antarctica, *Journal of Geophysical Research (Oceans)*, *113*(C12), 4039, doi:10.1029/2007JC004346.

Williams, G. D., M. Hindell, M. N. Houssais, T. Tamura, and I. C. Field (2011), Upper ocean stratification and sea ice growth rates during the summer-fall transition, as revealed by Elephant seal foraging in the Adélie Depression, East Antarctica, *Ocean Science*, *7*, 185–202, doi:10.5194/os-7-185-2011.

Wunsch, C., P. Heimbach, R. M. Ponte, I. Fukumori, E.-G. Consortium, et al. (2009), Global General Circulation of the Ocean Estimated by the ECCO-Consortium, *Oceanography*, *22*, 88–103.

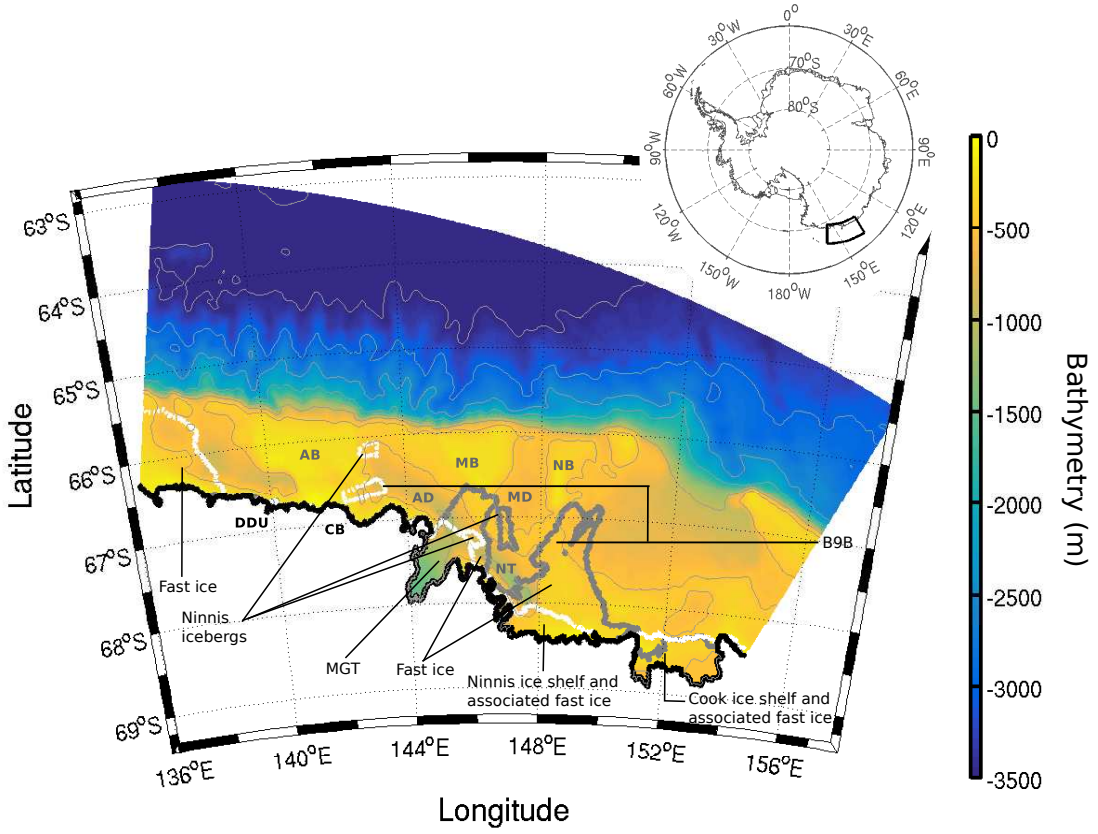

Figure S1. Bathymetry (in m) of the model overlaid with the model ice mask. Solid grey outline corresponds to the ice mask for the pre-calving simulation and the solid white outline corresponds to the ice mask for the post-calving simulation. The light grey contours are the bathymetry contours every 500 m on the continental shelf (until 1500 m) and every 1000 m for the deeper part of the model domain. Notable features referred to in the text are indicated. In the ocean: AB: Adélie Bank; AD: Adélie Depression; MB: Mertz Bank; MD: Mertz Depression; NT: Ninnis Trough. Along the continent: Commonwealth Bay (CB), and Dumont D'Urville station (DDU).

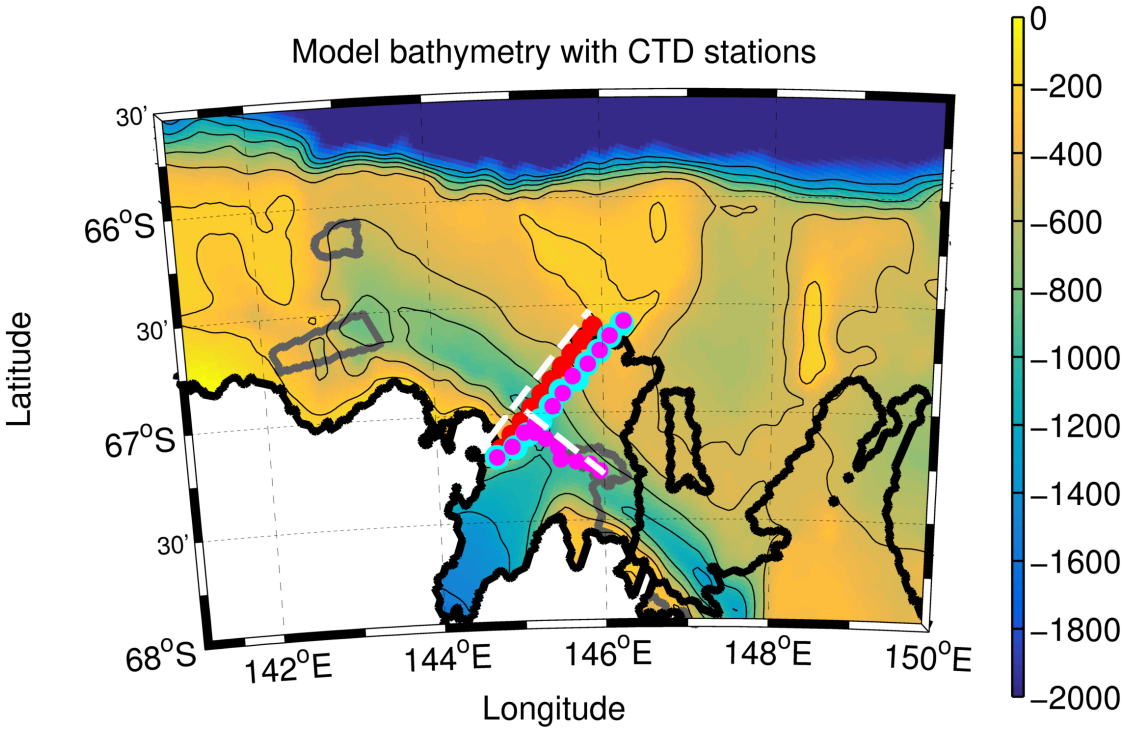

Figure S2. Model bathymetry (m) with bathymetry contours every 250 m. The black thick lines outline the coastline and the ice draft in the model. Conductivity-Temperature-Depth profiler (CTD) stations used to compare with the model are shown from 1999 (red), 2001 (cyan) and 2015 (magenta), along with the model sections used in the text (white dashed lines for MGT west and MGT north).

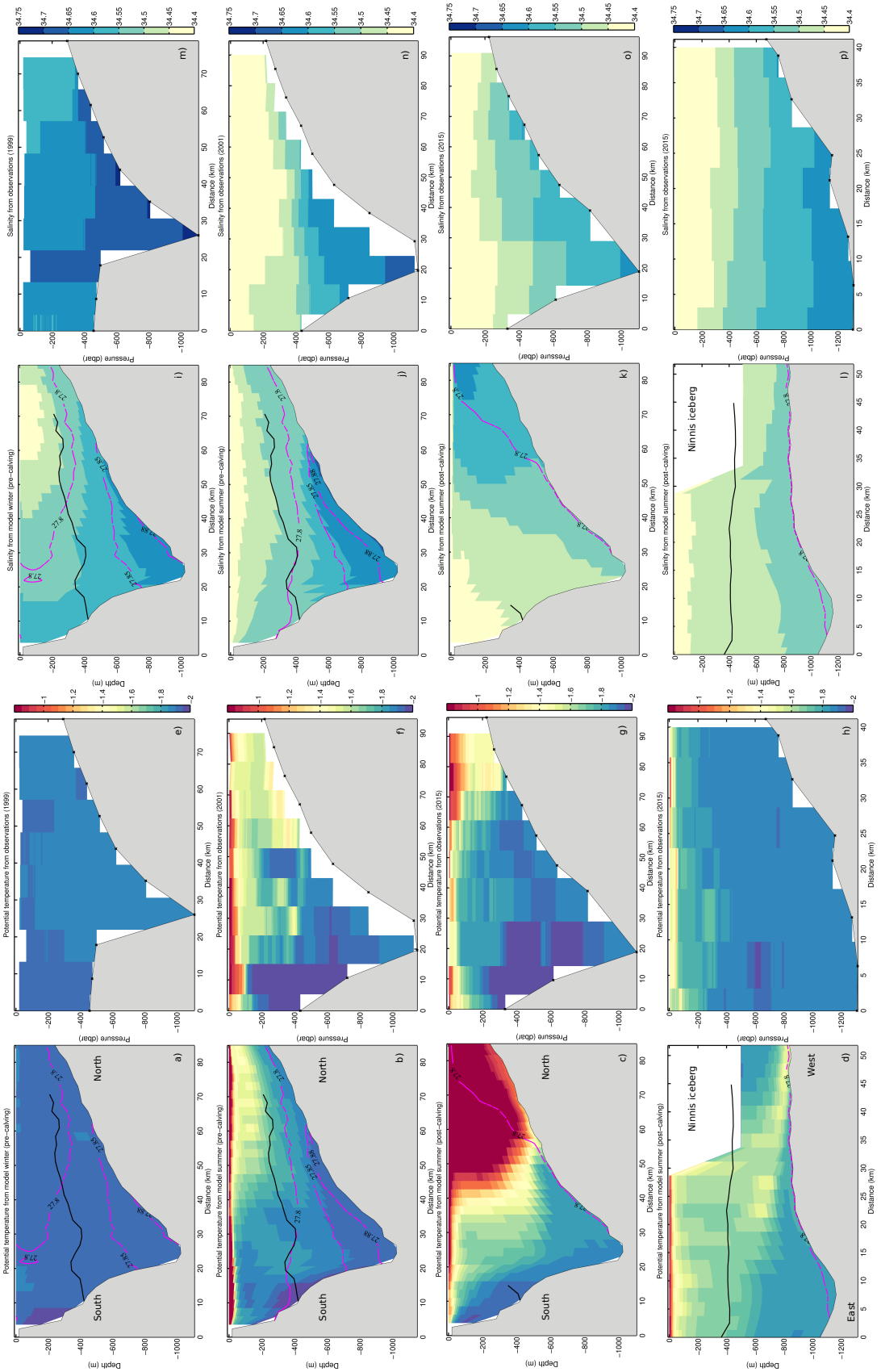

Figure S3. Potential temperature (°C: a-h) and salinity (i-p) sections, for the model simulations (a-d, i-l) and observations (e-h, m-p), along the MGT west section (a-c, e-g, i-k, m-o) and the MGT north (d, h, l, p). The black lines on the model panels outline the MGT ice draft at the closest from the section, and the magenta lines are the potential density contour from the model (kg m^{-3} -1000). The Ninnis iceberg is represented in white, it does not appear along the section from the observations as it moved in 2014 and the observations were taken in January 2015.

Table S1. Area-averaged basal melting and basal mass loss for the pre- and post-calving simulations with their standard deviation

Ice Shelf	Melt rate PRE (m yr^{-1})	Melt rate POST (m yr^{-1})	% area-averaged melt change	Mass loss PRE (Gt yr^{-1})	Mass loss POST (Gt yr^{-1})	% mass loss change	% basal ice shelf area change
Total [a]	0.88 ± 0.09	0.9 ± 0.2	+7	23.8 ± 2	20.5 ± 3	-14	-19
MGT	0.93 ± 0.08	1.7 ± 0.3	+89	5.6 ± 0.5	6.0 ± 1.0	+7	-42
B9B	2.2 ± 0.4	0.8 ± 0.1	-64	5.3 ± 0.9	0.6 ± 0.1	-89	-69
Ninnis	0.4 ± 0.3	0.8 ± 0.5	+100	0.6 ± 0.4	1.3 ± 0.8	+117	0
Cook	1.9 ± 0.4	1.2 ± 0.4	-37	7.3 ± 1.4	4.5 ± 1.7	-38	0
Fast ice (10 m)	0.3 ± 0.1	0.7 ± 0.1	+133	3.4 ± 1.0	6.7 ± 1.5	+94	+3
Fast ice (35 m)	0.26 ± 0.09	0.5 ± 0.5	+67	0.3 ± 0.1	0.2 ± 0.2	-33	-65
Other ice [b]	0.59 ± 0.06	0.8 ± 0.1	+42	1.2 ± 0.1	1.2 ± 0.2	0	
M^c < -900m	3.24 ± 0.08	5.1 ± 0.8	+57	2.16 ± 0.05	3.4 ± 0.5	+57	0
-900 < M^c < -600m	0.56 ± 0.02	1.1 ± 0.3	+95	0.86 ± 0.04	1.7 ± 0.5	+98	0
-600 < M^c < -300m	0.47 ± 0.06	0.7 ± 0.2	+49	1.2 ± 0.2	0.88 ± 0.3	-26	-50
M^c > -300m	1.1 ± 0.3	0.6 ± 0.3	-42	1.4 ± 0.4	0.009 ± 0.005	-99	-99

[a] All the ice in the model including all ice shelves, icebergs and fast ice

[b] Other ice refers to other icebergs and minor ice shelves in the domain

[c] MGT ice draft

Table S2. Area-averaged basal melt rate, friction velocity (u_*) and thermal forcing (T_*) for ice deeper than 600 m of the MGT

	pre-calving	post-calving	% of change [a]
Melt rate (m yr^{-1})	1.36 ± 1.7	2.30 ± 2.6	+69
T_* (°C)	0.26 ± 0.22	0.36 ± 0.28	+39
u_* (m s^{-1})	(38 ± 24) $\times 10^{-4}$	(48 ± 28) $\times 10^{-4}$	+26

[a] Percentage of change between the pre- and post-calving simulation